

This discussion paper is/has been under review for the journal Ocean Science (OS).  
Please refer to the corresponding final paper in OS if available.

# Recent transient tracer distributions in the Fram Strait: estimation of anthropogenic carbon content and transport

T. Stöven<sup>1</sup>, T. Tanhua<sup>1</sup>, M. Hoppema<sup>2</sup>, and W.-J. von Appen<sup>2</sup>

<sup>1</sup>Helmholtz Centre for Ocean Research Kiel, GEOMAR, Germany

<sup>2</sup>Alfred Wegener Institute Helmholtz Centre for Polar and Marine Research, Bremerhaven, Germany

Received: 5 August 2015 – Accepted: 24 August 2015 – Published: 24 September 2015

Correspondence to: T. Stöven (tstoeven@geomar.de)

Published by Copernicus Publications on behalf of the European Geosciences Union.

Title Page

Abstract

Introduction

Conclusions

References

Tables

Figures

◀

▶

◀

▶

Back

Close

Full Screen / Esc

Printer-friendly Version

Interactive Discussion



## Abstract

The storage of anthropogenic carbon in the ocean's interior is an important process which modulates the increasing carbon dioxide concentrations in the atmosphere. The polar regions are expected to be net sinks for anthropogenic carbon. Transport estimates of dissolved inorganic carbon and the anthropogenic offset can thus provide information about the magnitude of the corresponding storage processes.

Here we present a transient tracer, dissolved inorganic carbon (DIC) and total alkalinity (TA) data set along 78°50' N sampled in the Fram Strait in 2012. A theory on tracer relationships is introduced which allows for an application of the Inverse Gaussian - Transit Time Distribution (IG-TTD) at high latitudes and the estimation of anthropogenic carbon concentrations. Current velocity measurements along the same section were used to estimate the net flux of DIC and anthropogenic carbon through the Fram Strait.

The new theory explains the differences between the theoretical (IG-TTD based) tracer age relationship and the specific tracer age relationship of the field data by saturation effects during water mass formation and/or the deliberate release experiment of SF<sub>6</sub> in the Greenland Sea in 1996 rather than by different mixing or ventilation processes. Based on this assumption, a maximum SF<sub>6</sub> excess of 0.5–0.8 fmol kg<sup>-1</sup> was determined in the Fram Strait at intermediate depths (500–1600 m). The anthropogenic carbon concentrations are 50–55 μmol kg<sup>-1</sup> in the Atlantic Water/Recirculating Atlantic Water, 40–45 μmol kg<sup>-1</sup> in the Polar Surface Water/warm Polar Surface Water and between 10–35 μmol kg<sup>-1</sup> in the deeper water layers, with lowest concentrations in the bottom layer. The net DIC and anthropogenic carbon fluxes through the Fram Strait indicate a balanced exchange between the Arctic Ocean and the North Atlantic, although with high uncertainties.

OSD

12, 2189–2229, 2015

**C<sub>ant</sub> in the Fram Strait**

T. Stöven et al.

Title Page

Abstract

Introduction

Conclusions

References

Tables

Figures

◀

▶

◀

▶

Back

Close

Full Screen / Esc

Printer-friendly Version

Interactive Discussion



# 1 Introduction

Changes in the Arctic during the last decades stand in mutual relationship with changes in the adjacent ocean areas such as the Nordic Seas, the Atlantic and the Pacific Ocean. The elevated heat flux of warm Atlantic Water into the Arctic Ocean has, for example, significant influence on the perennial sea ice thickness and volume and thus on the fresh water input (Polyakov et al., 2005; Stroeve et al., 2008; Kwok et al., 2009; Kurtz et al., 2011). The exchange and transport of heat, salt and fresh water through the major gateways like Fram Strait, Barents Sea Opening, Canadian Archipelago and Bering Strait are also directly connected to changes in ventilation of the adjacent ocean areas (Wadley and Bigg, 2002; Vellinga et al., 2008; Rudels et al., 2012). The ventilation processes of the Arctic Ocean have a major impact on the anthropogenic carbon storage in the world ocean (Tanhua et al., 2008). Studying the fluxes of anthropogenic carbon through the major gateways contributes to the estimate of the integrated magnitude of such ocean–atmosphere interactions. It additionally provides information of a changing environment in the Arctic Mediterranean. The required flux data of the prevailing water masses, i.e. current velocity fields, are obtained by time series of long-term maintained mooring arrays in the different gateways. The Fram Strait is the deepest gateway to the Arctic Ocean with highest volume fluxes equatorwards and polewards. One of the well-established cross-section mooring arrays is located at  $\approx 78^{\circ}50' \text{ N}$  in the Fram Strait (Fahrbach et al., 2001; Schauer et al., 2008) which provided the basis for heat transport estimates in the past (Fahrbach et al., 2001; Schauer et al., 2004, 2008; Beszczynska-Möller et al., 2012). However, the current data interpretation and analysis of this mooring array is complicated due to a recirculation pattern and mesoscale eddy structures in this area (Schauer and Beszczynska-Möller, 2009; Rudels et al., 2008; Marnela et al., 2013; de Steur et al., 2014). The spatial and temporal volume flux variability and the insufficient instrument coverage in the deeper water layers, i.e. below the West Spitsbergen Current (WSC) and East Greenland Current (EGC), lead to high uncertainties of the net flux through Fram Strait. Hence, it is the

Title Page

Abstract

Introduction

Conclusions

References

Tables

Figures



Back

Close

Full Screen / Esc

Printer-friendly Version

Interactive Discussion



most relevant but also the most challenging gateway with respect to transport budgets in the Arctic Mediterranean.

Estimating an anthropogenic carbon budget presupposes the knowledge of the concentration ratio between the natural dissolved inorganic carbon (DIC) and the anthropogenic part ( $C_{\text{ant}}$ ) in the water column. An estimate of DIC transport across the Arctic Ocean boundaries is provided by MacGilchrist et al. (2014) who used velocity fields by Tsubouchi et al. (2012) and available DIC data. That work provides a proper estimate of DIC fluxes, although it does not separate the specific share of anthropogenic carbon and the uncertainties are relatively high. Here we present anthropogenic carbon column inventories in Fram Strait using a new data set of  $\text{SF}_6$  and CFC-12 along the cross-section of the mooring array at  $78^\circ 50' \text{ N}$  and a short meridional section along the fast ice edge in 2012. The anthropogenic carbon column inventories were estimated using the transient tracers and the Inverse Gaussian transit time distribution (IG-TTD) model. Flux estimates of DIC and anthropogenic carbon with the Atlantic Water, Recirculating/Return Atlantic Water and Polar Water water masses through Fram Strait are provided based on current velocities measured with moorings. Common error sources and specific aspects using these tracers and method in Fram Strait are highlighted.

## 2 Material and methods

### 2.1 Tracer and carbon data

A data set of CFC-12,  $\text{SF}_6$ , DIC and TA was obtained during the ARK-XXVII/1 expedition from 14 June to 15 July 2012 from Bremerhaven, Germany to Longyearbyen, Svalbard on the German research vessel *Polarstern* (Beszczynska-Möller, 2013). Figure 1 shows the stations of the zonal section along  $78^\circ 50' \text{ N}$ , where measurements of CFC-12,  $\text{SF}_6$ , DIC, and TA were conducted. The meridional section along the fast ice edge was only sampled for CFC-12 and  $\text{SF}_6$ .

OSD

12, 2189–2229, 2015

## $C_{\text{ant}}$ in the Fram Strait

T. Stöven et al.

Title Page

Abstract

Introduction

Conclusions

References

Tables

Figures

◀

▶

◀

▶

Back

Close

Full Screen / Esc

Printer-friendly Version

Interactive Discussion



[Title Page](#)[Abstract](#)[Introduction](#)[Conclusions](#)[References](#)[Tables](#)[Figures](#)[◀](#)[▶](#)[◀](#)[▶](#)[Back](#)[Close](#)[Full Screen / Esc](#)[Printer-friendly Version](#)[Interactive Discussion](#)

Water samples of the transient tracers CFC-12 and SF<sub>6</sub> were taken with 250 mL glass syringes and directly measured on board, using a purge and trap GC-ECD system similar to Law et al. (1994) and Bullister and Wisegarver (2008). The measurement system is identical to the “PT3” system described in Stöven and Tanhua (2014) except the cooling system and column composition. The trap consisted of a 1/16” column packed with 70 cm *Heysep D* and cooled to  $-70^{\circ}\text{C}$  during the purge process using a Dewar filled with a thin layer of liquid nitrogen. The 1/8” precolumn was packed with 30 cm *Porasil C* and 60 cm *Molsieve 5 Å* and the 1/8” main column with 180 cm *Carbograph 1AC*. Due to malfunctioning of the Electron Capture Detector (ECD) of the measurement system, the samples of 6 stations (between station 15 and 53) were taken with 300 mL glass ampules and flame sealed for later onshore measurements at GEOMAR. The onshore measurement procedure is described in Stöven and Tanhua (2014). The precision for the onshore measurements is  $\pm 4.4\%/0.09\text{ fmol kg}^{-1}$  for SF<sub>6</sub> and  $\pm 1.9\%/0.09\text{ pmol kg}^{-1}$  for CFC-12. The precision for onboard measurements is  $\pm 0.5\%/0.02\text{ fmol kg}^{-1}$  for SF<sub>6</sub> and  $\pm 0.6\%/0.02\text{ pmol kg}^{-1}$  for CFC-12.

The DIC and total alkalinity (TA) samples were taken with 500 mL glass bottles and poisoned with 100  $\mu\text{L}$  of a saturated mercuric chloride solution to prevent biological activities during storage time. The sampling procedure was carried out according to Dickson et al. (2007). The measurements of DIC and TA were performed onshore at the GEOMAR, using a coulometric measurement system (SOMMA) for DIC (Johnson et al., 1993, 1998) and a potentiometric titration (VINDTA) for TA (Mintrop et al., 2000). The precision is  $\pm 0.05\%/1.1\text{ }\mu\text{mol kg}^{-1}$  for DIC and  $\pm 0.08\%/1.7\text{ }\mu\text{mol kg}^{-1}$  for TA. The data of all obtained chemical parameters will be available at CDIAC by the end of 2015. The physical oceanographic data (temperature, salinity, and pressure) from the cruise where the tracers were measured can be found at Beszczynska-Möller and Wisotzki (2012).

## 2.2 Water transport data

An array of moorings across the deep Fram Strait from 9° E to 7° W has been maintained since 1997 by the Alfred Wegener Institute and the Norwegian Polar Institute. Since 2002, it has contained 17 moorings at 78°50' N. Here we use the gridded data from the array from summer 2002 to summer 2010 as described in Beszczynska-Möller et al. (2012). The more recent data has either not been recovered yet or the processing is still in progress. The moorings contained temperature and velocity sensors at five standard depths: 75, 250, 750, 1500, and 10m above the bottom. These hourly measurements were averaged to monthly values and then gridded onto a regular 5m vertical by 1000m horizontal grid using optimal interpolation. Since interannual trends are small (Beszczynska-Möller et al., 2012), we consider the long term average volume flux of the following water masses: Atlantic Water advected in the West Spitsbergen Current defined as longitude  $\geq 5^\circ$  E and depth  $\leq 750$  m; Recirculating and Return Atlantic Water which is both due to the recirculation of Atlantic Water in Fram Strait (de Steur et al., 2014) and the long loop of Atlantic Water through the Arctic Ocean (Karcher et al., 2012), defined as longitude  $\leq 5^\circ$  E, mean temperature  $\geq 1^\circ$  C, and depth  $\leq 750$  m; and finally Polar Water flowing southward in the East Greenland Current defined as mean temperature  $\leq 1^\circ$  C and depth  $\leq 750$  m. The estimate of the volume transport across Fram Strait below 750m from the moorings is more complicated. The method of Beszczynska-Möller et al. (2012) which was developed to study the fluxes in the West Spitsbergen Current predicts a net southward transport of 3.2Sv below 750m. This is unrealistic given that there are no connections between the Nordic Seas and the Arctic Ocean below the sill depth of the Greenland–Scotland Ridge (750m) other than Fram Strait. No vertical displacements of isopycnals in these two basins are observed that would suggest a non-zero net transport across Fram Strait below 750m (von Appen et al., 2015, in review). The large net transport inferred by Beszczynska-Möller et al. (2012) is due to errors and will be discussed in Sect. 3.6. For these reasons we assume a net flux of 0Sv across Fram Strait for the deep waters below 750m.

## 2.3 TTD method

A transit time distribution (TTD) model (Eq. 1) describes the propagation of a boundary condition into the interior of the ocean and is based on the Green's function (Hall and Plumb, 1994).

$$c(t_s, r) = \int_0^{\infty} c_0(t_s - t) e^{-\lambda t} \cdot G(t, r) dt \quad (1)$$

Here,  $c(t_s, r)$  is the specific tracer concentration at year  $t_s$  and location  $r$ ,  $c_0(t_s - t)$  the boundary condition described by the tracer concentration at source year  $t_s - t$  and  $G(t)$  the Green's function of the age spectra  $t$  of the tracer. The exponential term corrects for the decay rate of radioactive transient tracers. Eq. (2) provides a possible solution of the TTD model, based on a steady and one-dimensional advective velocity and diffusion gradient (Vaughan et al., 2003).

$$G(t) = \sqrt{\frac{\Gamma^3}{4\pi\Delta^2 t^3}} \cdot \exp\left(\frac{-\Gamma(t - \Gamma)^2}{4\Delta^2 t}\right) \quad (2)$$

It is known as the Inverse-Gaussian transit time distribution (IG-TTD) where  $G(t)$  is defined by the width of the distribution ( $\Delta$ ), the mean age ( $\Gamma$ ) and the age spectra of the tracer ( $t$ ). One can define a  $\Delta/\Gamma$  ratio of the IG-TTD which represents the proportion between the advective and diffusive properties of the mixing processes as included in the TTD. The lower the  $\Delta/\Gamma$  ratio, the higher is the advective share. A  $\Delta/\Gamma$  ratio of 1.0 is the commonly applied ratio at several tracer surveys (e.g. Vaughan et al., 2004, 2006; Tanhua et al., 2008; Schneider et al., 2010, 2014; Huhn et al., 2013). Here we also applied this unity ratio to the ARK-XXVII/1 data set.

The application of chlorofluorocarbons (CFCs) is restricted due to partly indistinct input functions to the ocean since the early 1990s. This is related to the recently decreasing atmospheric concentrations of CFCs. To this end, dichlorodifluoromethane

(CFC-12) data above the atmospheric concentration limit of 528 ppt in 2012 (Bullister, 2015) have no clear time information and are thus not applicable.

## 2.4 Anthropogenic carbon and the TTD

The IG-TTD model can be used to estimate the total amount of anthropogenic carbon in the water column (Waugh et al., 2004). For this purpose it is assumed that the anthropogenic carbon behaves like an inert passive tracer, i.e. similar to a transient tracer. Then applying Eq. (1), the concentration of anthropogenic carbon in the interior ocean ( $C_{\text{ant}}(t_s)$ ) is given by Eq. (3).

$$C_{\text{ant}}(t_s) = \int_{\infty}^0 C_{\text{ant},0}(t_s - t) \cdot G(r, t) dt \quad (3)$$

$C_{\text{ant},0}$  is the boundary condition of anthropogenic carbon at year  $t_s - t$  and  $G(r, t)$  the distribution function (see Eq. 1). The historic boundary conditions are described by the differences between the preindustrial and modern DIC concentrations at the ocean surface. These anthropogenic offsets can be calculated by applying the modern (elevated) partial pressures of  $\text{CO}_2$  and then subtracting the corresponding value of the preindustrial partial pressure. In each case, the preformed alkalinity was used as second parameter to determine the specific DIC concentrations (calculated using the Matlab version of the CO2SYS van Heuven et al., 2011). Here we assumed a constant  $p\text{CO}_{2,\text{water}}$  saturation in the surface. Since exact saturations are not well constrained, we present sensitivity calculations of different saturation states/disequilibria (see Sect. 3.6 below). The atmospheric history of  $p\text{CO}_{2,\text{atm}}$  is taken from Tans and Keeling (2015). The preformed alkalinity was determined by using the alkalinity/salinity relationship of MacGilchrist et al. (2014). This relationship is based on surface alkalinity and salinity measurements in Fram Strait which were corrected for sea-ice melt and formation processes.

The time dependent boundary conditions ( $C_{\text{ant},0}$ ) and Eq. (3) can then be used to calculate anthropogenic carbon concentrations ( $C_{\text{ant}}(t_s)$ ) and the corresponding mean

Title Page

Abstract

Introduction

Conclusions

References

Tables

Figures

◀

▶

◀

▶

Back

Close

Full Screen / Esc

Printer-friendly Version

Interactive Discussion



age. Finally, the mean age of Eq. (3) can be set in relation to the transient tracer based mean age of the water and allows for back-calculating  $C_{\text{ant}}(t_s)$ , i.e. it provides the link between the tracer concentration and the anthropogenic carbon concentration.

### 3 Results and discussion

#### 3.1 Water masses in Fram Strait

To highlight the different transient tracer characteristics we defined the water mass type of each sample by using the water mass properties suggested by Rudels et al. (2000, 2005) and the salinity and temperature data of this cruise from Beszczynska-Möller and Wisotzki (2012). Note that this water mass classification is not based on an optimum multiparameter analysis and only serves as an indication for this specific purpose.

Water masses of the Arctic Ocean are the Polar Surface Water (PSW) which is the cold and less saline surface and halocline water; the warm Polar Surface Water, defined by a potential temperature ( $\Theta$ )  $> 0$ , which comprises sea ice melt water due to interaction with warm Atlantic Water; the Arctic Atlantic Water/Return Atlantic Water which derives from sinking Atlantic Water due to cooling in the Arctic Ocean; the deep water masses are upper Polar Deep Water (uPDW), Canadian Basin Deep Water (CBDW) and Eurasian Basin Deep Water (EBDW). Deep water formation, e.g. on the Arctic shelves, usually involves densification from brine rejection. The Eurasian Basin Deep Water mixes with Greenland Sea Deep Water so that this layer corresponds to two sources in the Fram Strait (von Appen et al., 2015, in review).

Water masses of the Atlantic Ocean/Nordic Seas are the warm and saline Atlantic Water (AW) and the corresponding Recirculating Atlantic Water (RAW); the Arctic Intermediate Water which is mainly formed in the Greenland Sea; the Nordic Seas Deep Water which comprises Greenland Sea Deep Water (GSDW), Iceland Sea Deep Water (ISDW) and Norwegian Sea Deep Water (NSDW) and is formed by deep convection during winter time.



[Title Page](#)[Abstract](#)[Introduction](#)[Conclusions](#)[References](#)[Tables](#)[Figures](#)[Back](#)[Close](#)[Full Screen / Esc](#)[Printer-friendly Version](#)[Interactive Discussion](#)

Figure 2 shows the zonal water mass distribution in Fram Strait, which also includes the data from the fast-ice section. The surface layer is dominated by Atlantic Water and Recirculating Atlantic Water in the east and by Polar Surface Water in the west with a transition between 6° W and 4° E where Polar Surface Water overlays the Atlantic Water. Warm Polar Surface Water can be found within the Atlantic Water between 4–8° E. The Atlantic Water layer extends down to  $\approx$  600 m. Arctic Atlantic Water/Return Atlantic Water (AAW/RAAW) can be found at the upper continental slope of Greenland between 300–700 m. The intermediate layer between 500–1600 m consists mainly of Arctic Intermediate Water and, at the Greenland slope, partly of Upper Polar Deep Water. Canadian Basin Deep Water can be found between 1600–2400 m west of 4° E. Nordic Seas Deep Water is the prevailing water mass along the continental slope of Svalbard between 700–2400 m but can be also observed in the range of the Canadian Basin Deep Water layer. The Eurasian Basin Deep Water/Greenland Sea Deep Water forms the bottom layer below 2400 m.

### 3.2 Transient tracer and DIC distributions

Figure 3 shows the partial pressure of CFC-12 and SF<sub>6</sub> along the zonal section. Both tracers have significant concentrations through the entire water column and show a similar distribution pattern. The Atlantic Water shows a relatively homogeneous distribution of both tracers with CFC-12 partial pressures > 450 ppt and SF<sub>6</sub> partial pressures > 6 ppt. The Polar Surface Water at the shelf region shows a more distinct structure with partial pressures between 4–8 ppt of SF<sub>6</sub> and 410–560 ppt of CFC-12. The smaller concentration gradient of CFC-12 is related to the recently decreasing atmospheric concentration of CFC-12, which causes only slightly varying boundary conditions at the air–sea interface (see Sect. 2.3). The high-tracer concentration layer of the Polar Surface Water extends further eastwards as overlaying tongue of the Atlantic Water between 2–6° W. The intermediate layer between 500–1600 m is characterized by a clear tracer minimum along the continental slope of Greenland with partial pressures between 1.8–4.0 ppt of SF<sub>6</sub> and 150–350 ppt of CFC-12 and mainly comprises

[Title Page](#)
[Abstract](#)
[Introduction](#)
[Conclusions](#)
[References](#)
[Tables](#)
[Figures](#)
[Back](#)
[Close](#)
[Full Screen / Esc](#)
[Printer-friendly Version](#)
[Interactive Discussion](#)


Arctic Atlantic Water/Return Atlantic Water. East of this minimum, a remarkable tracer maximum can be observed at 1–3° W with partial pressures between 3–6ppt of SF<sub>6</sub> and 250–450ppt of CFC-12. A smaller maximum can be observed between 5–6° E at ≈ 1000 m with partial pressures of ≈ 5 ppt of SF<sub>6</sub> and ≈ 330 ppt of CFC-12. Both tracer maxima probably correspond to extensive ventilation events which mainly affected the Arctic Intermediate Water and partly the Atlantic Water in the transition zone of both water masses. The Arctic Intermediate Water in the Fram Strait thus consists of recently ventilated areas and less ventilated areas which is also indicated by the large range of transient tracer concentrations. The remaining intermediate layer above 1700 m is characterized by lower partial pressures between 2–3ppt of SF<sub>6</sub> and 150–300ppt of CFC-12 with decreasing concentrations with depth. This gradient extends throughout the deep water layers down to the bottom with partial pressures from 2ppt down to 0.2ppt of SF<sub>6</sub> and from 150ppt down to 34ppt of CFC-12. The fast-ice section is not presented here since it does not show any differences compared to the same longitude range of the zonal section.

Figure 4 shows the DIC concentrations along the zonal section separated into an upper and lower panel to highlight the different concentration ranges of the shallow and deep water layers. The Greenland shelf region shows concentrations between 1970 μmol kg<sup>-1</sup> in the surface and 2145 μmol kg<sup>-1</sup> at ≈ 200 m. The upper 200 m between 4–8° E shows increasing concentrations with depth between 2070 and 2155 μmol kg<sup>-1</sup>. There are three significant DIC maxima below 200 m. Two are located at the continental slope of Svalbard at 300–800 m and at 1400–2100 m with concentrations > 2158 μmol kg<sup>-1</sup> and a maximum concentration of 2167 μmol kg<sup>-1</sup>. The third maximum corresponds to the transient tracer maximum at 1–3° W but extends further eastwards with concentrations between 2158 and 2162 μmol kg<sup>-1</sup>. The area of the East Greenland Current at 3–8° W is characterized by concentrations between 2118 and 2152 μmol kg<sup>-1</sup>. The deep water below 1700 m shows concentrations between 2150 and 2158 μmol kg<sup>-1</sup>.

### 3.3 Transient tracers and the IG-TTD

The IG-TTD can be numerically constrained using transient tracer couples, CFC-12 and SF<sub>6</sub> in our case, which provides information about the mean age and the parameters of the IG-TTD (Waugh et al., 2002; Sonnerup et al., 2013; Stöven and Tanhua, 2014). The method of validity areas, introduced in Stöven et al. (2014), is used to determine the applicability of the tracer couple. For this purpose, the tracer age is calculated from the transient tracer concentrations (Waugh et al., 2003) which provides the tracer age relationship of the tracer couple. Figure 5 shows the tracer age relationship of our field data (colored by water mass) in relation to the range of theoretical tracer age relationships of the IG-TTD, i.e. for  $\Delta/\Gamma$  ratios between 0.1–1.8, which describe the range from advectively dominated to diffusively dominated water masses (grey shaded area). The black line in Fig. 5 denotes the tracer age relationship based on the unity ratio of  $\Delta/\Gamma = 1.0$ . Field data which corresponds to this unity ratio would be centered around the black line. The Fram Strait data can be separated into two branches of tracer age relationships. The upper branch consists of Atlantic Water/Recirculating Atlantic Water, Arctic Intermediate Water, Nordic Seas Deep Water, Eurasian Basin Deep Water/Greenland Sea Deep Water and Canadian Basin Deep Water whereas the lower branch consists of Polar Surface Water, warm Polar Surface Water, Arctic Atlantic Water/Return Atlantic Water and upper Polar Deep Water. The Polar Surface Water and warm Polar Surface Water can also partly be found in the upper branch for a SF<sub>6</sub> tracer age < 10 years. Note that the Arctic Atlantic Water/Return Atlantic Water and upper Polar Deep Water show a transition to the upper branch for a SF<sub>6</sub> tracer age larger than about 20 years. The data shows a more scattered and indistinct structure between 10 and 20 years of the SF<sub>6</sub> tracer age. However, the upper branch does not correspond to the unity ratio and, moreover, it is outside the validity area of the IG-TTD. Water masses related to the lower branch can be applied to the IG-TTD with tendencies towards higher  $\Delta/\Gamma$  ratios (> 1.0) since the data is clearly above the black line indicating a dominance of diffusive processes.

[Title Page](#)[Abstract](#)[Introduction](#)[Conclusions](#)[References](#)[Tables](#)[Figures](#)[Back](#)[Close](#)[Full Screen / Esc](#)[Printer-friendly Version](#)[Interactive Discussion](#)

Based on the raw field data, and on assumptions implemented in the IG-TTD (like 100 % saturation of the gases at the surface before entering deeper layers), the IG-TTD cannot describe the ventilation pattern of the different water masses in Fram Strait. Nevertheless, by comparing the shape of the two field data branches with the shape of the black line in Fig. 5, it is noted that both branches show similar characteristics as the unity ratio or, generally, as IG-TTD based tracer age relationships. This opens up the possibility to use the IG-TTD the other way around, i.e. to assume a fixed  $\Delta/\Gamma$  ratio to determine the deviation of transient tracer concentrations rather than using the transient tracer concentration to determine the  $\Delta/\Gamma$  ratio. Since several publications found the unity ratio of  $\Delta/\Gamma = 1.0$  to be valid in large parts of the ocean, we assumed that this is also true for water masses in Fram Strait. Figure 6 shows the mean tracer age relationship of the upper branch (red line) and the tracer age relationship of the unity ratio (black line/same as in Fig. 5). The offset of the field data related to the unity ratio suggests an undersaturation of CFC-12 and/or a supersaturation of SF<sub>6</sub> (see black box in Fig. 6). This uncommon coexistence of under- and supersaturated transient tracers is discussed in the following section.

### 3.4 Saturations and excess SF<sub>6</sub>

The surface saturations of transient tracers are influenced by sea surface temperature and salinity, ice coverage, wind speed, bubble effects, atmospheric growth rate of the tracer and the boundary dwell time of the water parcel (i.e. the time the water parcel is in contact with the atmosphere). However, the saturation state of transient tracers at the air–sea interface before, during and after water mass formation is rarely known, since water mass formation generally occurs in winter at high latitudes, which renders it almost impossible to obtain measurements. Shao et al. (2013) provide modelled data of monthly surface saturations of CFC-11, CFC-12 and SF<sub>6</sub> from 1936 to 2010 on a global scale. This model output can be used to estimate the tracer saturation ratio of different water masses by using the surface saturation of the specific formation area and yearly formation period. The formation types and areas are notably different for water masses

[Title Page](#)[Abstract](#)[Introduction](#)[Conclusions](#)[References](#)[Tables](#)[Figures](#)[Back](#)[Close](#)[Full Screen / Esc](#)[Printer-friendly Version](#)[Interactive Discussion](#)

that occur in Fram Strait. The model output shows high variabilities in surface saturations at different formation sites, namely the Greenland Sea, the Arctic shelf regions and the Arctic open water (Figs. 7 and 8). In contrast, the tracer age relationships of the two branches in Fig. 5 indicate relatively similar deviations in saturation. The complex boundary conditions in the Arctic, e.g. possible gas exchange through ice cover, might bias the results of the saturation model. Therefore, we only used the surface saturation of the Greenland Sea (Area 1 in Figs. 7 and 8) which agrees with the findings of Tanhua et al. (2008) who used available field data to investigate historic tracer saturations. The IG-TTD based mean age provides the link between the observed tracer concentrations and the corresponding time-dependent saturation factors. Therefore, the saturation factors were applied to the atmospheric history (boundary conditions) of each tracer. These new boundary conditions are then applied to the measured tracer concentrations and the IG-TTD which then yields a saturation-corrected mean age. This mean age in turn can then be used to back-calculate the saturation-corrected tracer concentrations using the originally (uncorrected) boundary conditions. We expect that undersaturation effects also hold for SF<sub>6</sub> but are counterbalanced by effects of supersaturation in this survey area.

The SF<sub>6</sub> excess is estimated using the corrected CFC-12 concentrations and the IG-TTD ( $\Delta/\Gamma = 1.0$ ) to calculate theoretical SF<sub>6</sub> concentrations of the water parcel, i.e. back-calculated SF<sub>6</sub> concentrations. The difference between the theoretical SF<sub>6</sub> concentration and the measured SF<sub>6</sub> concentration denotes the SF<sub>6</sub> excess in the water. Note that this SF<sub>6</sub> excess is based on the assumption that the IG-TTD and unity ratio describe the prevailing ventilation pattern of the water masses. Figure 9 shows the SF<sub>6</sub> excess in fmol kg<sup>-1</sup> and ppt for depths below 200m. This upper depth limit is invoked by the fact that CFC-12 concentrations above the current atmospheric concentration limit cannot be applied to the IG-TTD. The SF<sub>6</sub> excess is much higher (0.5–0.8 fmol kg<sup>-1</sup>/1.0–1.6 ppt) for northwards propagating water masses compared to water masses of Arctic origin (0–0.4 fmol kg<sup>-1</sup>/0–0.8 ppt). There are at least two possible effects which can cause such significant supersaturations of SF<sub>6</sub>.

[Title Page](#)[Abstract](#)[Introduction](#)[Conclusions](#)[References](#)[Tables](#)[Figures](#)[◀](#)[▶](#)[◀](#)[▶](#)[Back](#)[Close](#)[Full Screen / Esc](#)[Printer-friendly Version](#)[Interactive Discussion](#)

One possibility refers to the deliberate tracer release experiment in 1996 where 320 kg ( $\approx 2190$  mol) of SF<sub>6</sub> were introduced into the central Greenland Sea (Watson et al., 1999). The patch was redistributed by mixing processes and entered the Arctic Ocean via the Fram Strait and Barents Sea Opening and the North Atlantic via Denmark Strait and the Faroe Bank Channel (Olsson et al., 2005; Tanhua et al., 2005). Assuming that 50–80 % of the deliberately released SF<sub>6</sub> still remains in the Nordic Seas and the Arctic Ocean (1095–1752 mol) and that 10–50 % of the corresponding total volume of  $1.875 \times 10^{18}$ – $9.375 \times 10^{18}$  L (Eakins and Sharman, 2010) is affected, a mean offset of 0.12–0.93 fmol L<sup>-1</sup> is estimated. This mean offset is thus in the range of the observed SF<sub>6</sub> excess concentrations. However, CFC-12 and SF<sub>6</sub> data of the Southern Ocean (Stöven et al., 2014) shows similar tracer age relationships compared to the Fram Strait data but with no influence of deliberately released SF<sub>6</sub>. This indicates that probably an additional source of excess SF<sub>6</sub> exists.

Liang et al. (2013) introduced a model which estimates supersaturations of dissolved gases by bubble effects in the ocean. This model predicted an increasing supersaturation for increasing wind speed and decreasing temperature, i.e. the bubble effect becomes more significant at high latitudes. Furthermore, Liang et al. (2013) show that the magnitude of supersaturation depends on the solubility of the gas. The less soluble a gas, the more supersaturation can be expected. Supporting this, Stöven et al. (2014) describe surface measurements of SF<sub>6</sub> and CFC-12 directly after heavy wind conditions in the Southern Ocean where SF<sub>6</sub> supersaturations between 20–50 % could be observed. The CFC-12 concentrations were only affected to a minor extent which indeed seems to be explained by the differences in solubility. This bubble induced supersaturation can also be expected to apply during the process of water mass formation in the Greenland Sea which usually occurs during late winter, i.e. during a period with low surface temperatures and heavy wind conditions. Furthermore, looking at the maximum SF<sub>6</sub> excess in the Arctic Intermediate Water layer in Fig. 9 and the generally elevated tracer concentrations of CFC-12 and SF<sub>6</sub> in the same area (see Fig. 3) reaffirms the assumption of bubble induced supersaturation of SF<sub>6</sub>. However, this hy-

pothesis stands in opposition to the current assumption that trace gases are generally undersaturated during water mass formation (Tanhua et al., 2008; Shao et al., 2013).

Future investigations are necessary to determine the different impact of under- and supersaturation effects on soluble gases at the air–sea interface. It can be expected that possible scenarios are not restricted to distinct saturation states anymore but rather comprise mixtures of equilibrated, under- and supersaturated states of the different gases.

### 3.5 Anthropogenic carbon and mean age

Since CFC-12 is not affected by tracer release experiments and possibly only to minor extent by bubble effects we used this tracer to calculate the mean age of the water and the corresponding anthropogenic carbon content. SF<sub>6</sub> was only used in the surface and upper halocline, i.e. where CFC-12 exceeds the atmospheric concentration limit of 528 ppt and where effects of SF<sub>6</sub> supersaturation are comparatively small. Saturation-corrected tracer data was applied for subsurface data below 100m whereas surface data was found to be near equilibrium state with the atmosphere. Figure 10 shows the anthropogenic carbon distribution in  $\mu\text{mol kg}^{-1}$  and Fig. 11 shows the mean age of the water masses. According to the relation between transient tracers, mean age and anthropogenic carbon, the distribution patterns are similar as for the transient tracers. The highest anthropogenic carbon concentrations of 50–55  $\mu\text{mol kg}^{-1}$  can be found in the upper 600 m of the Atlantic Water/Recirculating Atlantic Water and a little lower concentrations of 40–45  $\mu\text{mol kg}^{-1}$  in the Polar Surface Water/warm Polar Surface Water layer. The mean age of these water masses is between 0–20 years. Note that these water layers show the highest mean current velocities in Fram Strait (see Sect. 3.7 below). The area of the tracer maximum at 1–3° W shows elevated concentrations of 35–40  $\mu\text{mol kg}^{-1}$  and a mean age of 20–40 years. The remaining water layers below 600 m show anthropogenic carbon concentrations lower than 35  $\mu\text{mol kg}^{-1}$  with decreasing concentrations with increasing depth and is comparatively low ( $< 10 \mu\text{mol kg}^{-1}$ ) in deep water masses such as Canadian Basin Deep Water and Eurasian Basin Deep Wa-

ter/Greenland Sea Deep Water. Accordingly, the mean age increases with increasing depth from 30 to 280 years and shows a maximum mean age of 286 years in the bottom layer at the prime meridian. Table 1 shows the mean values and standard deviation of each specific water layer.

The determined values correspond to the findings of Jutterström and Jeansson (2008) who used a similar method to determine anthropogenic carbon of the East Greenland Current in 2002. The Fram Strait section of their data set shows a similar distribution pattern of anthropogenic carbon but with lower concentration levels compared to our data from 2012. The concentration differences indicate an increase of the anthropogenic carbon content between 25–35 % in the entire water column during the elapsed ten years. This corresponds to an increase of  $2 \mu\text{mol kg}^{-1} \text{yr}^{-1}$  in the Atlantic Water,  $1 \mu\text{mol kg}^{-1} \text{yr}^{-1}$  in the Polar Water and between  $0.5\text{--}1 \mu\text{mol kg}^{-1} \text{yr}^{-1}$  in the deeper water layers. Based on these current rates of increase it can be assumed that the import of anthropogenic carbon by Atlantic Water becomes more dominant compared to the export by Polar Water.

### 3.6 Sensitivities on anthropogenic carbon

The calculations presented above are based on the ideal case of  $p\text{CO}_{2,\text{atm}} = p\text{CO}_{2,\text{water}}$  at the sea surface before entering the ocean interior, and the assumption that the saturation correction of the tracers and the unity ratio of the IG-TTD are true for water masses in the Fram Strait. Since the three parameters involved cannot be directly determined it is very likely that deviations from the ideal case exist. Therefore we present the corresponding sensitivities in the following. The sensitivities are determined by changing only one parameter and keeping the others constant at ideal conditions.

Figure 12a and b shows the sensitivities of changes in tracer saturation using the example of CFC-12 since most of the anthropogenic carbon calculations are based on this tracer. Small deviations of  $\pm 5\%$  in CFC-12 saturations cause only small deviations of anthropogenic carbon concentrations of  $\pm 1 \mu\text{mol kg}^{-1} / \pm 2\text{--}4\%$ . Furthermore, the sensitivity depends on the partial pressure range of CFC-12. The lower the partial

Title Page

Abstract

Introduction

Conclusions

References

Tables

Figures

◀

▶

◀

▶

Back

Close

Full Screen / Esc

Printer-friendly Version

Interactive Discussion



pressure the less sensitive is the anthropogenic carbon concentrations to changes in CFC-12 saturation. The maximum deviations are  $\pm 6 \mu\text{mol kg}^{-1} / \pm 11\text{--}16\%$  for partial pressure  $> 400$  ppt. The white patches in Fig. 12a and b corresponds to supersaturations which exceed the atmospheric concentration limit of CFC-12.

Figure 12c and d shows the sensitivities due to changes in the  $\Delta/\Gamma$  ratio of the IG-TTD. The sensitivity is very low ( $< 1 \mu\text{mol kg}^{-1} / < 5\%$ ) for most of the ratio and concentration range. Partial pressures below 100 ppt and  $\Delta/\Gamma < 0.4$  show the highest sensitivity with deviations between  $5\text{--}10 \mu\text{mol kg}^{-1} / 50\text{--}200\%$ . The unusual sensitivity distribution is related to the indistinct boundary condition of CFC-12 in recent years and the distribution function of the TTD. For more information see Stöven et al. (2014).

The sensitivities of deviations in  $p\text{CO}_2$  saturations are shown in Fig. 12e and f. The absolute error is characterized by a relatively steady change with changing saturation states. The absolute error is more or less independent of the partial pressure of CFC-12 and leads to maximum deviations of  $\pm 20\text{--}25 \mu\text{mol kg}^{-1}$ . The relative error (0–200 %) shows an increasing sensitivity of anthropogenic carbon concentrations to changes in  $p\text{CO}_2$  saturations and decreasing CFC-12 partial pressures. Note that a negative deviation of 100 % corresponds to a anthropogenic carbon concentration of  $0 \mu\text{mol kg}^{-1}$  which is also indicated by the turning-points where the contour lines continue parallel to the  $x$  axis in Fig. 12e. This indicates that small uncertainties in  $p\text{CO}_2$  saturations can cause large errors in anthropogenic carbon estimates for low tracer concentrations, i.e. for a high mean age of the water. The uncertainty of the  $p\text{CO}_2$  saturation remains as the largest error source although the saturation of  $p\text{CO}_2$  and CFC-12 counteract each other.

### 3.7 Carbon transport estimates

Table 2 shows the transport estimates of DIC and anthropogenic carbon separated into northwards propagating (positive values) and southwards propagating (negative values) water masses. The northwards flux comprises the Atlantic Water of the West Spitsbergen Current, the southwards flux comprises the Recirculating/Return Atlantic

Title Page

Abstract

Introduction

Conclusions

References

Tables

Figures

◀

▶

◀

▶

Back

Close

Full Screen / Esc

Printer-friendly Version

Interactive Discussion



Water and the Polar Water of the East Greenland Current. The mean flux of deep water layers below 750 m was taken to be 0 Sv and therefore not considered for this estimate. The water masses were defined as described in Sect. 2.2.

The northwards flux transports  $3420 \pm 2497 \text{ Tg C yr}^{-1}$  (mean  $\pm$  standard deviation) of DIC and  $82 \pm 59 \text{ Tg C yr}^{-1}$  of anthropogenic carbon into the Arctic Ocean. This input is counterbalanced by an export of  $2274 \pm 5080 \text{ Tg C yr}^{-1} / 54 \pm 120 \text{ Tg C yr}^{-1}$  by Recirculating and Return Atlantic Water and  $1117 \pm 660 \text{ Tg C yr}^{-1} / 23 \pm 13 \text{ Tg C yr}^{-1}$  by Polar Water. The carbon transport uncertainties are relatively high, especially with respect to the error range of the Recirculating/Return water masses of the Atlantic Water. Furthermore, there is a lack of water transport data on the Greenland shelf region, e.g. Belgica Bank, and thus we cannot with great confidence decide whether more anthropogenic carbon is transported into or out of the Arctic region through the Fram Strait.

### 3.8 Uncertainties

The applicability of IG-TTD model at high latitudes, like in the Fram Strait or the Southern Ocean, is supposed to be limited by complex water mass mixing and ventilation patterns. They should rather be described by more refined models like the maximum entropy method by Holzer and Primeau (2012). The main uncertainty factor is related to the assumption that different saturation states of the transient tracers are responsible for the tracer age relationships rather than specific mixing processes and that thereby the IG-TTD model is valid for all water masses in the Fram Strait. The uncertainties of the IG-TTD model depend on the shape of the IG-TTD, i.e. the  $\Delta/\Gamma$  ratio, and the uncertainties of the boundary conditions and the measurement precision of the transient tracers and apparent transient tracers (see Sect. 3.6 above). The flux estimates are based on transient tracer and DIC data of the ARK-XXVII/1 cruise which only show the specific distribution pattern during June/July 2012 and thus neglect any interannual variabilities of the parameters. The determination of the preformed alkalinity highly depends on the used method. Here we used the linear relationship between surface alkalinity and salinity which is a commonly used method. However, other au-

thors recommend the use of data from the subsurface layer (Vazquez-Rodriguez et al., 2012) or the surface temperature and salinity dependencies (Lee et al., 2006).

The transport estimates are complicated by the fact that the flow field in Fram Strait is dominated by many small scale features. The Rossby radius is 4–6 km which means that the mooring spacing is only able to fully resolve the mesoscale near the shelfbreak in the West Spitsbergen Current. Otherwise, eddies may be aliased between the moorings. The velocities in the recirculation area in the center of Fram Strait are actually mostly westward (Beszczynska-Möller et al., 2012) and thus along the mooring array line. Therefore, the meridional velocities in the center of Fram Strait are only the small residuals of much larger zonal velocities. As a result the finite accuracy and precision of the current direction measurements has a big impact on the meridional exchanges. Additionally, at depth the flow is topographically steered, but the topographic features are also not fully resolved. Interannual variations are also neglected here, but they are small (Beszczynska-Möller et al., 2012). The exchange flow across Fram Strait below 750 m (sill depth of Greenland–Scotland ridge and depth horizon of the third instruments on the moorings) is assumed to be 0 Sv for the present purpose.

## 4 Conclusions

Measurements of the transient tracers CFC-12 and SF<sub>6</sub> along 78°50' N in the Fram Strait in 2012 show specific characteristics of the different water masses. The tracer age relationship between both tracers can be separated into two major branches. One branch describes the tracer age relationship of water masses of Atlantic origin as well as deep water masses, the other describes water masses of Arctic origin. We assumed that the different tracer age relationships are due to different saturation effects on the tracers during water mass formation and still existing offsets of the SF<sub>6</sub> concentrations caused by the deliberate tracer release experiment in the Greenland Sea in 1996. The CFC-12 data was saturation corrected by applying the model output of Shao et al. (2013). The corrected data was used to back-calculate theoretical SF<sub>6</sub> data based on

OSD

12, 2189–2229, 2015

C<sub>ant</sub> in the Fram Strait

T. Stöven et al.

Title Page

Abstract

Introduction

Conclusions

References

Tables

Figures

◀

▶

◀

▶

Back

Close

Full Screen / Esc

Printer-friendly Version

Interactive Discussion



the IG-TTD which then provides the excess concentrations of SF<sub>6</sub>. The largest excess concentrations of 0.5–0.8 fmol kg<sup>-1</sup> were found for the intermediate layer between 500 m and 1600 m.

The anthropogenic carbon content was estimated using the IG-TTD and saturation-corrected CFC-12 data in the ocean interior (depths below 100 m) and SF<sub>6</sub> in the surface layer. The Atlantic Water and Recirculating Atlantic Water is characterized by anthropogenic carbon concentrations of 50–55 μmol kg<sup>-1</sup> and the Polar Surface Water by concentrations of 40–45 μmol kg<sup>-1</sup>. Maximum concentrations of 35–40 μmol kg<sup>-1</sup> in the intermediate layer can be found at 1–3° W. Deep water layers show decreasing concentrations with increasing depth from 35 μmol kg<sup>-1</sup> down to ≈ 10 μmol kg<sup>-1</sup>.

The mean current velocity data obtained by a mooring-array at 78°50' N between 2002 and 2010 suggests a mean northwards flux of 4.2 (±3.0) Sv of Atlantic Water (West Spitsbergen Current) and a mean southward flux of 2.8 (±6.2) Sv of Recirculating/Return Atlantic Water and 1.4 (±0.8) Sv of Polar Water (East Greenland Current). The net flux of water masses below 750 m was taken to be 0 Sv. The high uncertainties of the flux data in the Fram Strait inhibit any statements about dominating shares of DIC and anthropogenic exports or imports to the Arctic Ocean. However, the flux estimates indicate a balanced transport budget with a northward flux of 3420 (±2497) Tg C yr<sup>-1</sup> of DIC and 82 (±59) Tg C yr<sup>-1</sup> of anthropogenic carbon by Atlantic Water and a southward flux of 2274 (±5080) Tg C yr<sup>-1</sup> / 54 (±120) Tg C yr<sup>-1</sup> by Recirculating and Return Atlantic Water and 1117 (±660) Tg C yr<sup>-1</sup> / 23 (±13) Tg C yr<sup>-1</sup> by Polar Water.

*Acknowledgements.* This work was supported by the Deutsche Forschungsgemeinschaft (DFG) in the framework of the priority programme “Antarctic Research with comparative investigations in Arctic ice areas” by a grant to T. Tanhua and M. Hoppema: Carbon and transient tracers dynamics: A bi-polar view on Southern Ocean eddies and the changing Arctic Ocean (TA 317/5, HO 4680/1). Partial support to T. Tanhua and M. Hoppema was received from EU FP7 project CARBOCHANGE “Changes in carbon uptake and emissions by oceans in a changing climate” (European Community’s 7th Framework Programme, grant agreement no. 264879). We are grateful to the Alfred-Wegener-Institut for participation in Polarstern cruise ARK-XXVII/1. We are happy to acknowledge the great support by the master and crew of

Polarstern, the chief scientist and the scientific party. Special thanks goes to Boie Bogner for his technical support during the ARK-XXVII/1 cruise.

The article processing charges for this open-access publication were covered  
5 by a Research Centre of the Helmholtz Association.

## References

Beszczyńska-Möller, A.: The expedition of the research vessel Polarstern to the Arctic in 2012 (ARK-XXVII/1), Reports on Polar and Marine Research, 660, 1–78, doi:10.2312/BzPM\_0660\_2013, 2013. 2192

10 Beszczyńska-Möller, A. and Wisotzki, A.: Physical Oceanography During POLARSTERN Cruise ARK-XXVII/1, Alfred-Wegener-Institute, Helmholtz Center for Polar and Marine Research, Bremerhaven, doi:10.1594/PANGAEA.801791, 2012. 2193, 2197

Beszczyńska-Möller, A., Fahrbach, E., Schauer, U., and Hansen, E.: Variability in Atlantic water temperature and transport at the entrance to the Arctic Ocean, 1997-2010, ICES J. Mar. Sci.,  
15 69, 852–863, 2012. 2191, 2194, 2208

Bullister, J.: Atmospheric Histories (1765–2015) for CFC-11, CFC-12, CFC-113, CCl<sub>4</sub>, SF<sub>6</sub> and N<sub>2</sub>O, Carbon Dioxide Information Analysis Center, Oak Ridge National Laboratory, US Department of Energy, Oak Ridge, Tennessee, USA, doi:10.3334/CDIAC/otg.CFC\_ATM\_Hist\_2015, 2015. 2196

20 Bullister, J. L. and Wisegarver, D.: The shipboard analysis of trace levels of sulfur hexafluoride, chlorofluorocarbon-11 and chlorofluorocarbon-12 in seawater, Deep-Sea Res. Pt. I, 55, 1063–1074, 2008. 2193

de Steur, L., Hansen, E., Mauritzen, C., Beszczyńska-Möller, A., and Fahrbach, E.: Impact of recirculation on the East Greenland Current in Fram Strait: Results from moored current meter measurements between 1997 and 2009, Deep-Sea Res., 92, 26–40, 2014. 2191,  
25 2194

Dickson, A., Sabine, C., and Chrisitan, J.: Guide to Best Practices for Ocean CO<sub>2</sub> Measurements, in: Guide to best practices for ocean CO<sub>2</sub> measurements, edited by: Dickson, A. G., Sabine, C. L., and Christian, J. R., PICES Special Publication 3, 2007. 2193

Title Page

Abstract

Introduction

Conclusions

References

Tables

Figures

◀

▶

◀

▶

Back

Close

Full Screen / Esc

Printer-friendly Version

Interactive Discussion



**C<sub>ant</sub> in the Fram Strait**

T. Stöven et al.

Title Page

Abstract

Introduction

Conclusions

References

Tables

Figures

◀

▶

◀

▶

Back

Close

Full Screen / Esc

Printer-friendly Version

Interactive Discussion



- Eakins, B. and Sharman, G.: Volumes of the World's Ocean from ETOPO1, NOAA National Geophysical Data Center, Boulder, CO, USA, available at: [http://ngdc.noaa.gov/mgg/global/etopo1\\_ocean\\_volumes.html](http://ngdc.noaa.gov/mgg/global/etopo1_ocean_volumes.html) (last access: 22 September 2015), 2010. 2203
- Fahrbach, E., Meincke, J., Østerhus, S., Rohardt, G., Schauer, U., Tverberg, V., and Verduin, J.: Direct measurements of volume transports through Fram Strait, *Polar Res.*, 20, 217–224, doi:10.1111/j.1751-8369.2001.tb00059.x, 2001. 2191
- Hall, T. M. and Plumb, R. A.: Age as a diagnostic of stratospheric transport, *J. Geophys. Res.*, 99, 1059–1070, 1994. 2195
- Holzer, M. and Primeau, F. W.: Improved constraints on transit time distributions from argon 39: A maximum entropy approach, *J. Geophys. Res.-Oceans*, 115, C12021, doi:10.1029/2010JC006410, 2012. 2207
- Huhn, O., Rhein, M., Hoppema, M., and van Heuven, S.: Decline of deep and bottom water ventilation and slowing down of anthropogenic carbon storage in the Weddell Sea, 1984–2011, *Deep-Sea Res. Pt. I*, 76, 66–84, doi:10.1016/j.dsr.2013.01.005, 2013. 2195
- Johnson, K., Wills, K., Butler, D., Johnson, W., and Wong, C.: Coulometric total carbon dioxide analysis for marine studies: maximizing the performance of an automated gas extraction system and coulometric detector, *Mar. Chem.*, 44, 167–187, doi:10.1016/0304-4203(93)90201-X, 1993. 2193
- Johnson, K. M., Dickson, A. G., Eiseheid, G., Goyet, C., Guenther, P., Key, R. M., Millero, F. J., Purkerson, D., Sabine, C. L., Schottle, R. G., Wallace, D. W., Wilke, R. J., and Winn, C. D.: Coulometric total carbon dioxide analysis for marine studies: assessment of the quality of total inorganic carbon measurements made during the US Indian Ocean CO<sub>2</sub> Survey 1994–1996, *Mar. Chem.*, 63, 21–37, doi:10.1016/S0304-4203(98)00048-6, 1998. 2193
- Jutterström, S. and Jeansson, E.: Anthropogenic carbon in the East Greenland Current, *Prog. Oceanogr.*, 78, 29–36, doi:10.1016/j.pocean.2008.04.001, 2008. 2205
- Karcher, M., Smith, J. N., Kauker, F., Gerdes, R., and Smethie, W. M.: Recent changes in Arctic Ocean circulation revealed by iodine-129 observations and modeling, *J. Geophys. Res.-Oceans*, 117, C08007, doi:10.1029/2011JC007513, 2012. 2194
- Kurtz, N., Markus, T., Farrell, S., Worthen, D., and Boisvert, L.: Observations of recent Arctic sea ice volume loss and its impact on ocean-atmosphere energy exchange and ice production, *J. Geophys. Res.-Oceans*, 116, C04015, doi:10.1029/2010JC006235, 2011. 2191

[Title Page](#)[Abstract](#)[Introduction](#)[Conclusions](#)[References](#)[Tables](#)[Figures](#)[Back](#)[Close](#)[Full Screen / Esc](#)[Printer-friendly Version](#)[Interactive Discussion](#)

- Kwok, R., Cunningham, G., Wensnahan, M., Rigor, I., Zwally, H., and Yi, D.: Thinning and volume loss of the Arctic Ocean sea ice cover: 2003-2008, *J. Geophys. Res.-Oceans*, 114, C07005, doi:10.1029/2009JC005312, 2009. 2191
- Law, C. S., Watson, A. J., and Liddicoat, M. I.: Automated vacuum analysis of sulphur hexafluoride in seawater: derivation of the atmospheric trend (1970-1993) and potential as a transient tracer, *Mar. Chem.*, 48, 57–69, 1994. 2193
- Lee, K., Tong, L., Millero, F., Sabine, C., Dickson, A., Goyet, C., Park, G., Wanninkhof, R., Feely, R., and Key, R.: Global relationships of total alkalinity with salinity and temperature in surface waters of the worlds oceans, *Geophys. Res. Lett.*, 33, L19605, doi:10.1029/2006GL027207, 2006. 2208
- Liang, J.-H., Deutsch, C., McWilliams, J. C., Baschek, B., Sullivan, P. P., and Chiba, D.: Parameterizing bubble-mediated air-sea gas exchange and its effect on ocean ventilation, *Global Biogeochem. Cy.*, 27, 894–905, doi:10.1002/gbc.20080, 2013. 2203
- MacGilchrist, G., Naveira Garabato, A., Tsubouchi, T., Bacon, S., Torres-Valdes, S., and Azetsu-Scott, K.: The Arctic Ocean carbon sink, *Deep-Sea Res. Pt. I*, 86, 39–55, doi:10.1016/j.dsr.2014.01.002, 2014. 2192, 2196
- Marnela, M., Rudels, B., Houssais, M.-N., Beszczynska-Möller, A., and Eriksson, P. B.: Recirculation in the Fram Strait and transports of water in and north of the Fram Strait derived from CTD data, *Ocean Sci.*, 9, 499–519, doi:10.5194/os-9-499-2013, 2013. 2191
- Mintrop, L., Pérez, F. F., González-Dávila, M., Santana-Casiano, J. M., Körtzinger, A.: Alkalinity determination by potentiometry: intercalibration using three different methods, *Cienc. Mar.*, 26, 23–37, 2000. 2193
- Olsson, K. A., Jeansson, E., Tanhua, T., and Gascard, J.-C.: The East Greenland Current studied with CFCs and released sulphur hexafluoride, *J. Marine Syst.*, 55, 77–95, doi:10.1016/j.jmarsys.2004.07.019, 2005. 2203
- Polyakov, I., Beszczynska, A., Carmack, E., Dmitrenko, I., Fahrbach, E., Frolov, I., Gerdes, R., Hansen, E., Holfort, J., Ivanov, V., Johnson, M., Karcher, M., Kauker, F., Morison, J., Orvik, K. A., Schauer, U., Simmons, H., Skagseth, Ø., Sokolov, V., Steele, M., Timokhov, L., Walsh, D., and Walsh, J.: One more step toward a warmer Arctic, *Geophys. Res. Lett.*, 32, L17605, doi:10.1029/2005GL023740, 2005. 2191
- Rudels, B., Meyer, R., Fahrbach, E., Ivanov, V. V., Østerhus, S., Quadfasel, D., Schauer, U., Tverberg, V., and Woodgate, R. A.: Water mass distribution in Fram Strait and over the

Title Page

Abstract

Introduction

Conclusions

References

Tables

Figures

◀

▶

◀

▶

Back

Close

Full Screen / Esc

Printer-friendly Version

Interactive Discussion



Yermak Plateau in summer 1997, *Ann. Geophys.*, 18, 687–705, doi:10.1007/s00585-000-0687-5, 2000. 2197

Rudels, B., Björk, G., Nilsson, J., Winsor, P., Lake, I., and Nohr, C.: The interaction between waters from the Arctic Ocean and the Nordic Seas north of Fram Strait and along the East Greenland Current: results from the Arctic Ocean-02 Oden expedition, *J. Marine Syst.*, 55, 1–30, doi:10.1016/j.jmarsys.2004.06.008, 2005. 2197

Rudels, B., Marnela, M., and Eriksson, P.: Constraints on estimating mass, heat and freshwater transports in the Arctic Ocean: an exercise, in: *Arctic-Subarctic Ocean Fluxes*, edited by: Dickson, R., Meincke, J., and Rhines, P., Springer Netherlands, 315–341, doi:10.1007/978-1-4020-6774-7\_14, 2008. 2191

Rudels, B., Korhonen, M., Budéus, G., Beszczynska-Möller, A., Schauer, U., Nummelin, A., Quadfasel, D., and Valdimarsson, H.: The East Greenland Current and its impacts on the Nordic Seas: observed trends in the past decade, *ICES J. Mar. Sci.*, 69, 841–851, doi:10.1093/icesjms/fss079, 2012. 2191

Schauer, U. and Beszczynska-Möller, A.: Problems with estimation and interpretation of oceanic heat transport – conceptual remarks for the case of Fram Strait in the Arctic Ocean, *Ocean Sci.*, 5, 487–494, doi:10.5194/os-5-487-2009, 2009. 2191

Schauer, U., Fahrbach, E., Østerhus, S., and Rohardt, G.: Arctic warming through the Fram Strait: oceanic heat transport from 3 years of measurements, *J. Geophys. Res.-Oceans*, 109, C06026, doi:10.1029/2003JC001823, 2004. 2191

Schauer, U., Beszczynska-Möller, A., Walczowski, W., Fahrbach, E., Piechura, J., and Hansen, E.: Variation of measured heat flow through the Fram Strait between 1997 and 2006, in: *Arctic-Subarctic Ocean Fluxes*, edited by: Dickson, R., Meincke, J., and Rhines, P., Springer Netherlands, 65–85, doi:10.1007/978-1-4020-6774-7\_4, 2008. 2191

Schneider, A., Tanhua, T., Koertzinger, A., and Wallace, D.: High anthropogenic carbon content in the eastern Mediterranean, *J. Geophys. Res.*, 115, C12050, doi:10.1029/2010JC006171, 2010. 2195

Schneider, A., Tanhua, T., Roether, W., and Steinfeldt, R.: Changes in ventilation of the Mediterranean Sea during the past 25 year, *Ocean Sci.*, 10, 1–16, doi:10.5194/os-10-1-2014, 2014. 2195

Shao, A. E., Mecking, S., Thompson, L., and Sonnerup, R. E.: Mixed layer saturations of CFC-11, CFC-12, and SF6 in a global isopycnal model, *J. Geophys. Res.-Oceans*, 118, 4978–4988, doi:10.1002/jgrc.20370, 2013. 2201, 2204, 2208, 2225

**C<sub>ant</sub> in the Fram Strait**

T. Stöven et al.

Title Page

Abstract

Introduction

Conclusions

References

Tables

Figures



Back

Close

Full Screen / Esc

Printer-friendly Version

Interactive Discussion



- Sonnerup, R., Mecking, S., and Bullister, J.: Transit time distributions and oxygen utilization rates in the Northeast Pacific Ocean from chlorofluorocarbons and sulfur hexafluoride, *Deep-Sea Res. Pt. I*, 72, 61–71, doi:10.1016/j.dsr.2012.10.013, 2013. 2200
- Stöven, T. and Tanhua, T.: Ventilation of the Mediterranean Sea constrained by multiple transient tracer measurements, *Ocean Sci.*, 10, 439–457, doi:10.5194/os-10-439-2014, 2014. 2193, 2200
- Stöven, T., Tanhua, T., Hoppema, M., and Bullister, J. L.: Perspectives of transient tracer applications and limiting cases, *Ocean Sci.*, 11, 699–718, doi:10.5194/os-11-699-2015, 2015. 2200, 2203, 2206
- Stroeve, J., Serreze, M., Drobot, S., Gearheard, S., Holland, M., Maslanik, J., Meier, W., and Scambos, T.: Arctic sea ice extent plummets in 2007, *EOS T. Am. Geophys. Un.*, 89, 13–14, doi:10.1029/2008EO020001, 2008. 2191
- Tanhua, T., Bulsiewicz, K., and Rhein, M.: Spreading of Overflow Water from the Greenland to the Labrador Sea, *Geophys. Res. Lett.*, 32, L10605, doi:10.1029/2005GL022700, 2005. 2203
- Tanhua, T., Waugh, D. W., and Wallace, D. W. R.: Use of SF<sub>6</sub> to estimate anthropogenic CO<sub>2</sub> in the upper ocean, *J. Geophys. Res.*, 113, 2156–2202, doi:10.1029/2007JC004416, 2008. 2191, 2195, 2202, 2204
- Tans, P. and Keeling, R.: Full Mauna Loa CO<sub>2</sub> record, NOAA/ESRL, available at: [www.esrl.noaa.gov/gmd/ccgg/trends/](http://www.esrl.noaa.gov/gmd/ccgg/trends/), last access: 22 September, 2015. 2196
- Tsubouchi, T., Bacon, S., Naveira Garabato, A. C., Aksenov, Y., Laxon, S. W., Fahrbach, E., Beszczynska-Möller, A., Hansen, E., Lee, C. M., and Ingvaldsen, R. B.: The Arctic Ocean in summer: a quasi-synoptic inverse estimate of boundary fluxes and water mass transformation, *J. Geophys. Res.-Oceans*, 117, C01024, doi:10.1029/2011JC007174, 2012. 2192
- van Heuven, S., Pierrot, D., Rae, J., Lewis, E., and Wallace, D.: MATLAB Program Developed for CO<sub>2</sub> System Calculations, Carbon Dioxide Information Analysis Center, Oak Ridge National Laboratory, US Department of Energy, Oak Ridge, Tennessee, USA, doi:10.3334/CDIAC/otg.CO2SYS\_MATLAB\_v1.1, 2011. 2196
- Vazquez-Rodriguez, M., Padin, X., Pardo, P., Rios, A., and Perez, F.: The subsurface layer reference to calculate preformed alkalinity and air-sea CO<sub>2</sub> disequilibrium in the Atlantic Ocean, *J. Marine Syst.*, 94, 52–63, 2012. 2208
- Vellinga, M., Dickson, B., and Curry, R.: The changing view on how freshwater impacts the Atlantic meridional overturning circulation, in: *Arctic-Subarctic Ocean Fluxes*, edited by: Dick-

**C<sub>ant</sub> in the Fram Strait**

T. Stöven et al.

Title Page

Abstract

Introduction

Conclusions

References

Tables

Figures



Back

Close

Full Screen / Esc

Printer-friendly Version

Interactive Discussion



son, R., Meincke, J., and Rhines, P., Springer Netherlands, 289–313, doi:10.1007/978-1-4020-6774-7\_13, 2008. 2191

von Appen, W.-J., Schauer, U., Cabrillo, R. S., Bauerfeind, E., and Beszczynska-Möller, A.: Exchange of warming deep waters across Fram Strait, *Deep-Sea Res.*, 103, 86–100, doi:10.1016/j.dsr.2015.06.003, 2015. 2194, 2197

Wadley, M. and Bigg, G.: Impact of flow through the Canadian Archipelago and Bering Strait on the North Atlantic and Arctic circulation: an ocean modelling study, *Q. J. Roy. Meteor. Soc.*, 128, 2187–2203, doi:10.1256/qj.00.35, 2002. 2191

Watson, A., Messias, M., Fogelqvist, E., Scoy, K. V., Johannessen, T., Oliver, K., Stevens, D., Rey, F., Tanhua, T., Olsson, K., Carse, F., Simonsen, K., Ledwell, J., Jansen, E., Cooper, D., Kruepke, J., and Guilyardi, E.: Mixing and convection in the Greenland Sea from a tracer-release experiment, *Nature*, 401, 902–904, doi:10.1038/44807, 1999. 2203

Waugh, D. W., Vollmer, M. K., Weiss, R. F., Haine, T. W. N., and Hall, T. M.: Transit time distributions in Lake Issyk-Kul, *Geophys. Res. Lett.*, 29, 84-1–84-4, doi:10.1029/2002GL016201, 2002. 2200

Waugh, D. W., Hall, T. M., and Haine, T. W. N.: Relationships among tracer ages, *J. Geophys. Res.*, 108, C01024, doi:10.1029/2002JC001325, 2003. 2195, 2200

Waugh, D. W., Haine, T. W. N., and Hall, T. M.: Transport times and anthropogenic carbon in the subpolar North Atlantic Ocean, *Deep-Sea Res. Pt. I*, 51, 1475–1491, 2004. 2195, 2196

Waugh, D. W., Hall, T. M., McNeil, B. I., Key, R., and Matear, R. J.: Anthropogenic CO<sub>2</sub> in the oceans estimated using transit time distributions, *Tellus B*, 58, 376–389, 2006. 2195

**C<sub>ant</sub> in the Fram Strait**

T. Stöven et al.

Title Page

Abstract

Introduction

Conclusions

References

Tables

Figures

◀

▶

◀

▶

Back

Close

Full Screen / Esc

Printer-friendly Version

Interactive Discussion



**Table 1.** Mean ( $\pm$  standard deviation) concentrations of anthropogenic carbon ( $C_{\text{ant}}$ ) and mean age in Fram Strait separated in water mass types.

Water mass	$C_{\text{ant}}$ [ $\mu\text{mol kg}^{-1}$ ]	Mean age [years]
AW/RAW	50 ( $\pm 6$ )	9 ( $\pm 10$ )
PSWw	46 ( $\pm 5$ )	9 ( $\pm 10$ )
PSW	43 ( $\pm 2$ )	7 ( $\pm 6$ )
AAW/RAAW	38 ( $\pm 5$ )	32 ( $\pm 15$ )
AIW	31 ( $\pm 5$ )	54 ( $\pm 20$ )
uPDW	28 ( $\pm 4$ )	69 ( $\pm 19$ )
NDW	18 ( $\pm 4$ )	143 ( $\pm 44$ )
CBDW	15 ( $\pm 2$ )	173 ( $\pm 23$ )
EBDW/GSDW	11 ( $\pm 1$ )	254 ( $\pm 32$ )

**C<sub>ant</sub> in the Fram Strait**

T. Stöven et al.

Title Page

Abstract

Introduction

Conclusions

References

Tables

Figures



Back

Close

Full Screen / Esc

Printer-friendly Version

Interactive Discussion

**Table 2.** Flux estimates of DIC and anthropogenic carbon in Fram Strait in 2012.

	Volume [Sv]	Transport [TgCyr <sup>-1</sup> ]	
		DIC	Anthropogenic carbon
AW	4.2 (±3.0)	3420 (±2497)	82 (±59)
RAW/RAAW	-2.8 (±6.2)	-2274 (±5080)	-54 (±120)
PW	-1.4 (±0.8)	-1117 (±660)	-23 (±13)
Σ	0	29	5

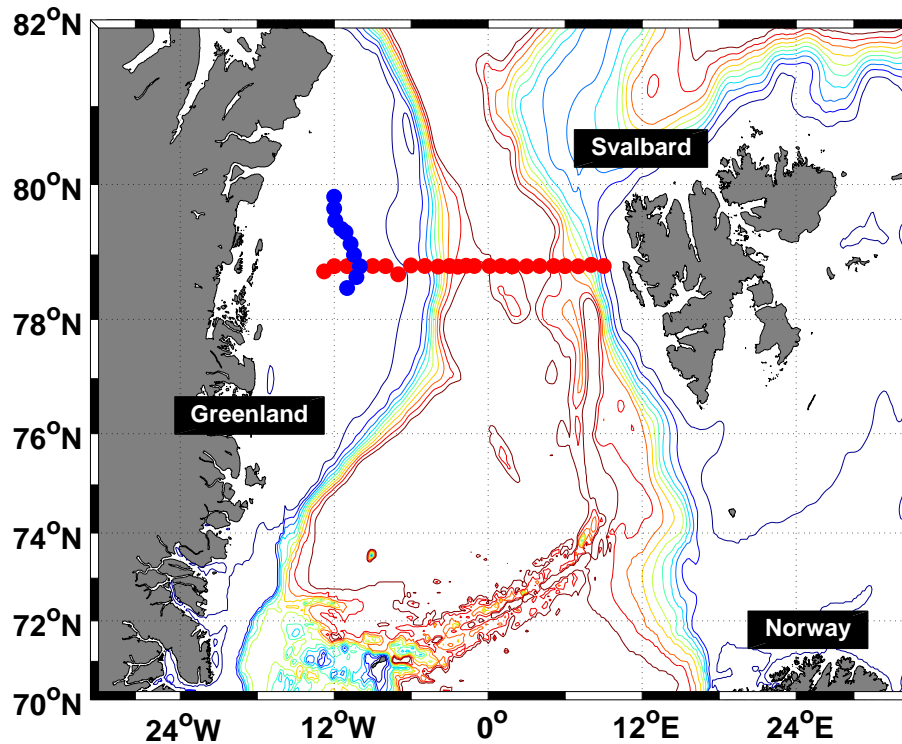


**Figure 1.** Sample stations of the ARK-XXVII/1 cruise in 2012. The zonal stations are highlighted as red dots and the meridional stations along the fast ice edge as blue dots. The depth contours are 250 : 250 : 2500.

Title Page	
Abstract	Introduction
Conclusions	References
Tables	Figures
◀	▶
◀	▶
Back	Close
Full Screen / Esc	
Printer-friendly Version	
Interactive Discussion	



**C<sub>ant</sub> in the Fram Strait**

T. Stöven et al.

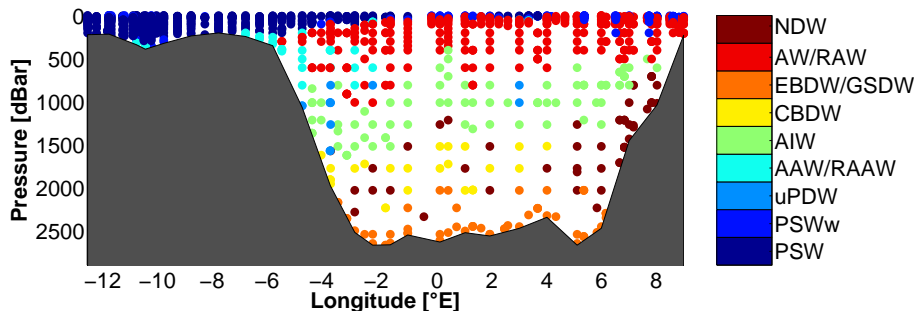


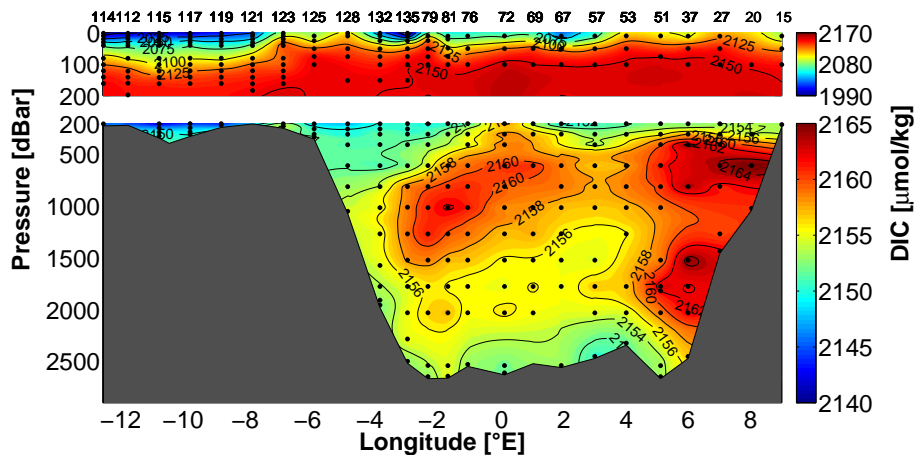
**Figure 2.** Water masses in Fram Strait: Nordic Seas Deep Water (NDW), Atlantic Water/Recirculating Atlantic Water (AW/RAW), Eurasian Basin Deep Water (EBDW)/Greenland Sea Deep Water (GSDW), Canadian Basin Deep Water (CBDW), Arctic Intermediate Water (AIW), Arctic Atlantic Water (AAW)/Return Atlantic Water (RAAW), Upper Polar Deep Water (uPDW), Polar Surface Water warm (PSWw) and Polar Surface Water (PSW).

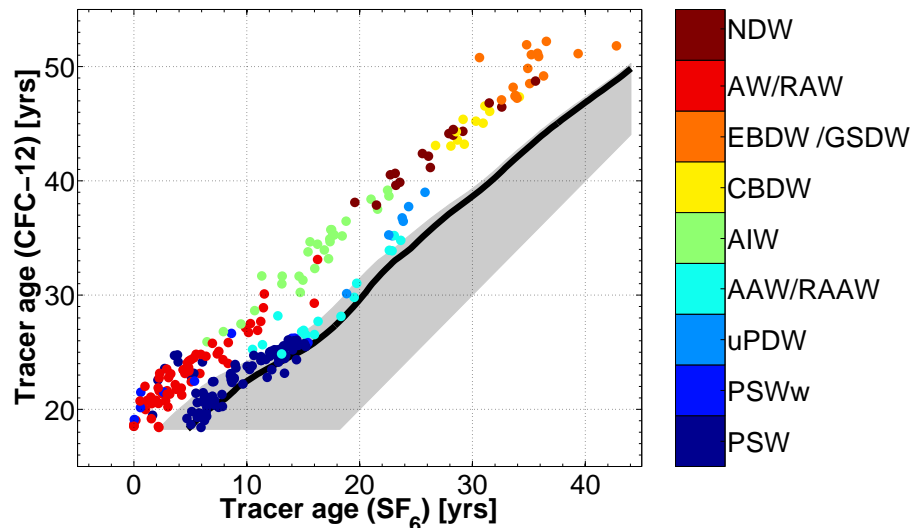
[Title Page](#)[Abstract](#)[Introduction](#)[Conclusions](#)[References](#)[Tables](#)[Figures](#)[◀](#)[▶](#)[◀](#)[▶](#)[Back](#)[Close](#)[Full Screen / Esc](#)[Printer-friendly Version](#)[Interactive Discussion](#)



**C<sub>ant</sub> in the Fram Strait**

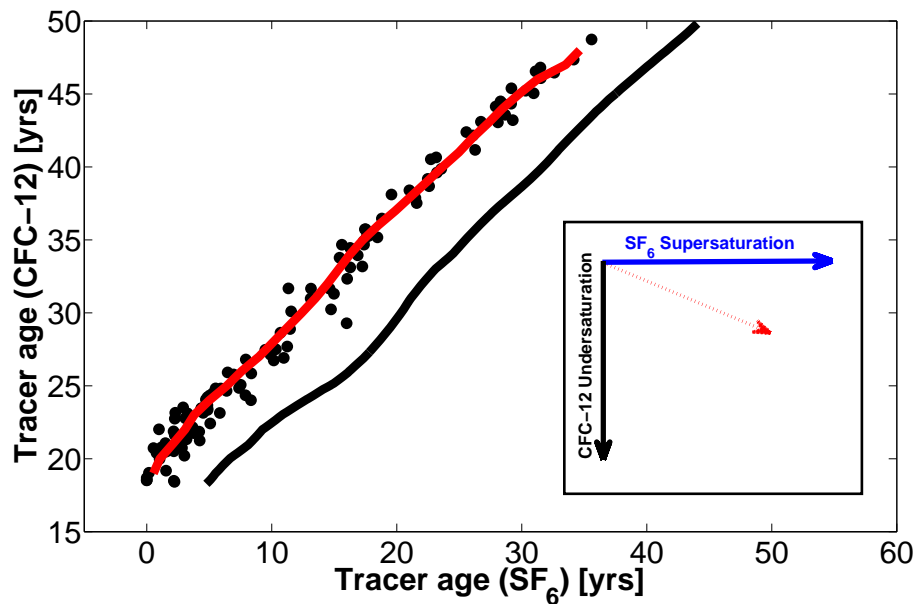
T. Stöven et al.

**Figure 4.** Dissolved inorganic carbon (DIC) in  $\mu\text{mol kg}^{-1}$ .[Title Page](#)[Abstract](#)[Introduction](#)[Conclusions](#)[References](#)[Tables](#)[Figures](#)[◀](#)[▶](#)[◀](#)[▶](#)[Back](#)[Close](#)[Full Screen / Esc](#)[Printer-friendly Version](#)[Interactive Discussion](#)



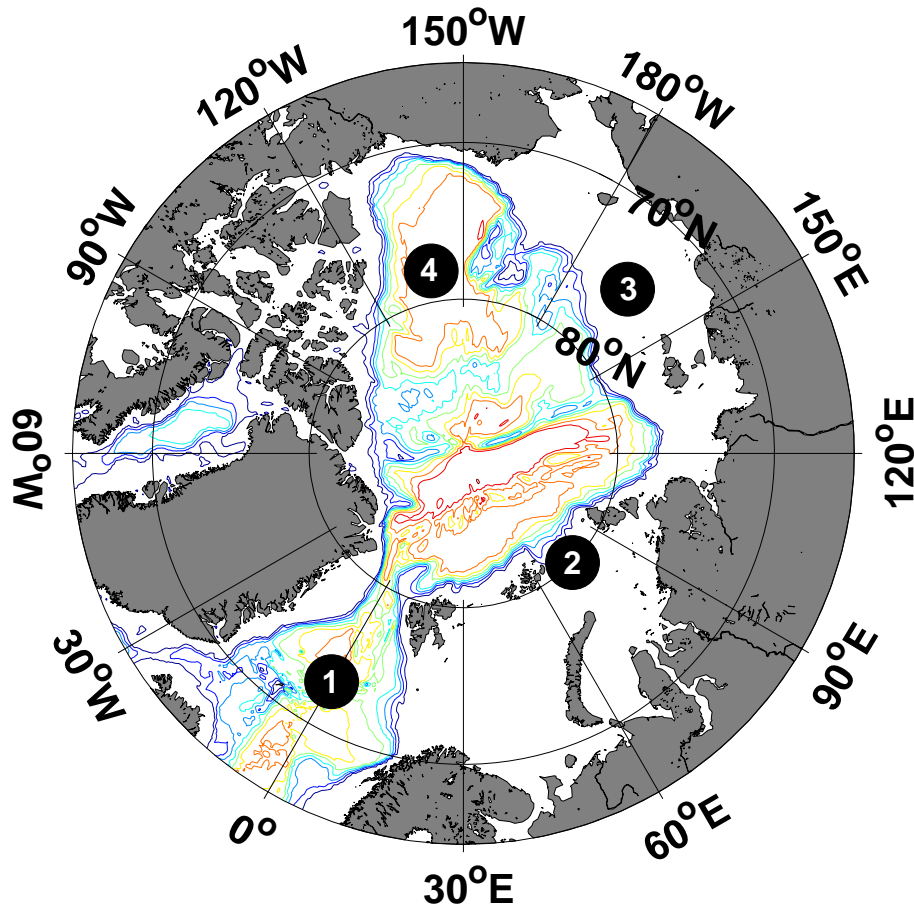
**Figure 5.** Validity area of the IG-TTD defined by the tracer couple CFC-12 and SF<sub>6</sub> (grey shaded area). The black line indicates the IG-TTD based tracer age relationship using the unity ratio of  $\Delta/\Gamma = 1.0$ . The field data is colored by the type of water mass. The lower branch (blue dots) describes surface and intermediate water of Arctic origin whereas the upper branch includes water of Atlantic origin and deep water masses.

[Title Page](#)
[Abstract](#)
[Introduction](#)
[Conclusions](#)
[References](#)
[Tables](#)
[Figures](#)
[◀](#)
[▶](#)
[◀](#)
[▶](#)
[Back](#)
[Close](#)
[Full Screen / Esc](#)
[Printer-friendly Version](#)
[Interactive Discussion](#)

**Figure 6.** Relation between the IG-TTD based tracer age relationship of the unity ratio (black line) and the mean tracer age relationship of the upper branch of the field data (red line). The shape of both curves indicates similarities between the modelled and field data. The difference can be explained by undersaturation of CFC-12 and/or supersaturation of SF<sub>6</sub> (see inset).

[Title Page](#)[Abstract](#)[Introduction](#)[Conclusions](#)[References](#)[Tables](#)[Figures](#)[◀](#)[▶](#)[◀](#)[▶](#)[Back](#)[Close](#)[Full Screen / Esc](#)[Printer-friendly Version](#)[Interactive Discussion](#)



**Figure 7.** Typical source regions of different water mass types. (1) the Greenland Sea, (2–3) Arctic shelf regions and (4) Arctic open water/fast-ice region.

Title Page

Abstract

Introduction

Conclusions

References

Tables

Figures

◀

▶

◀

▶

Back

Close

Full Screen / Esc

Printer-friendly Version

Interactive Discussion



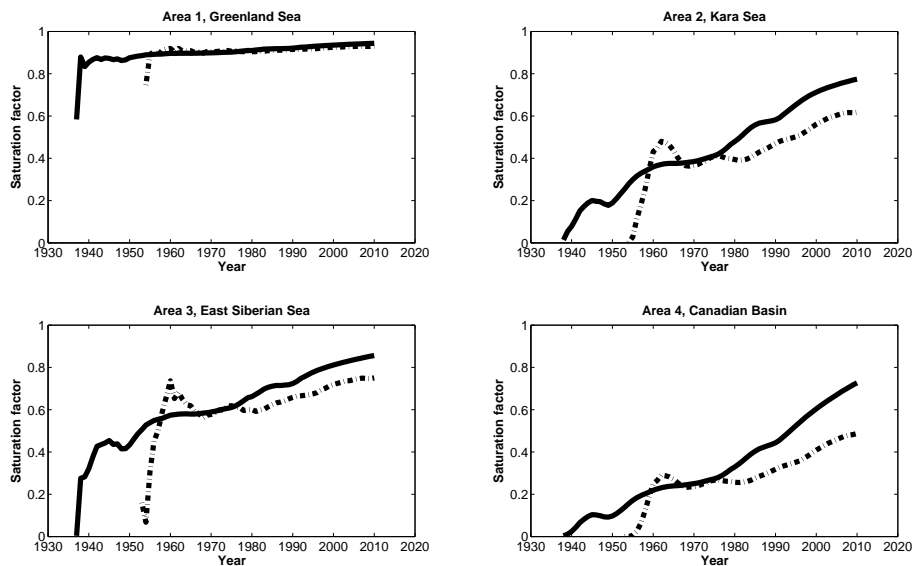


**Figure 8.** Surface saturation of CFC-12 (black solid line) and SF<sub>6</sub> (black dash-dotted line) of different source regions (see Fig. 7) based on the model output of Shao et al. (2013). The data shows mean values of the corresponding grids with a dimension of 300 nm × 300 nm.

[Title Page](#)[Abstract](#)[Introduction](#)[Conclusions](#)[References](#)[Tables](#)[Figures](#)[◀](#)[▶](#)[◀](#)[▶](#)[Back](#)[Close](#)[Full Screen / Esc](#)[Printer-friendly Version](#)[Interactive Discussion](#)



**C<sub>ant</sub> in the Fram Strait**

T. Stöven et al.

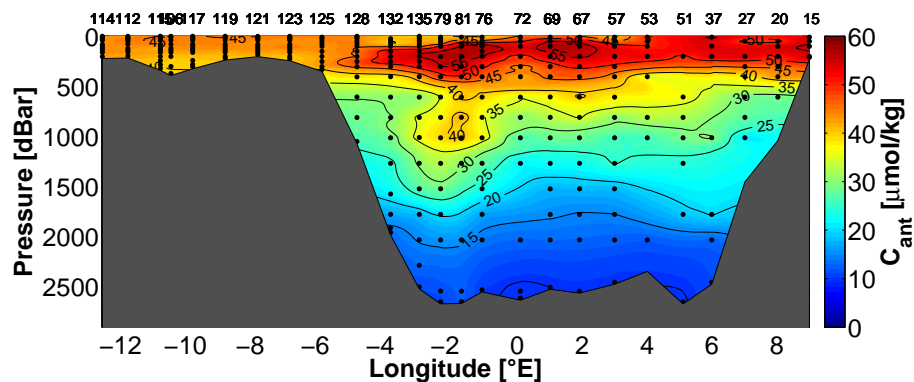


**Figure 10.** Anthropogenic carbon in  $\mu\text{mol kg}^{-1}$ .

[Title Page](#)[Abstract](#)[Introduction](#)[Conclusions](#)[References](#)[Tables](#)[Figures](#)[◀](#)[▶](#)[◀](#)[▶](#)[Back](#)[Close](#)[Full Screen / Esc](#)[Printer-friendly Version](#)[Interactive Discussion](#)

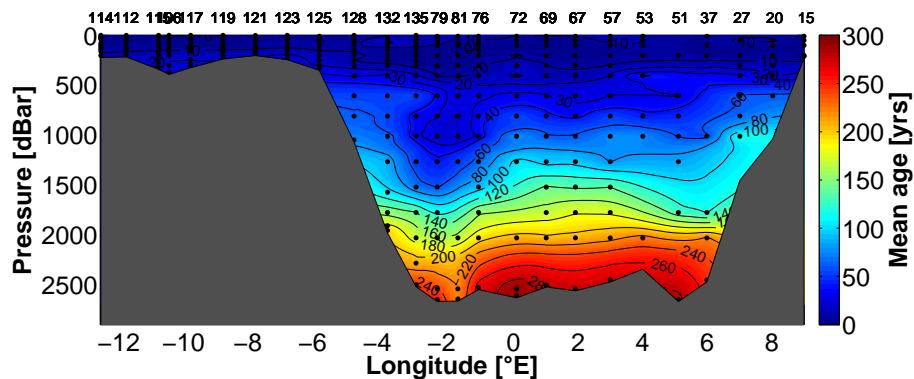


**Figure 11.** Mean age based on saturation corrected CFC-12 data below 100 m and SF<sub>6</sub> data in shallower depths.

[Title Page](#)[Abstract](#)[Introduction](#)[Conclusions](#)[References](#)[Tables](#)[Figures](#)[◀](#)[▶](#)[◀](#)[▶](#)[Back](#)[Close](#)[Full Screen / Esc](#)[Printer-friendly Version](#)[Interactive Discussion](#)

Title Page

Abstract

Introduction

Conclusions

References

Tables

Figures



Back

Close

Full Screen / Esc

Printer-friendly Version

Interactive Discussion

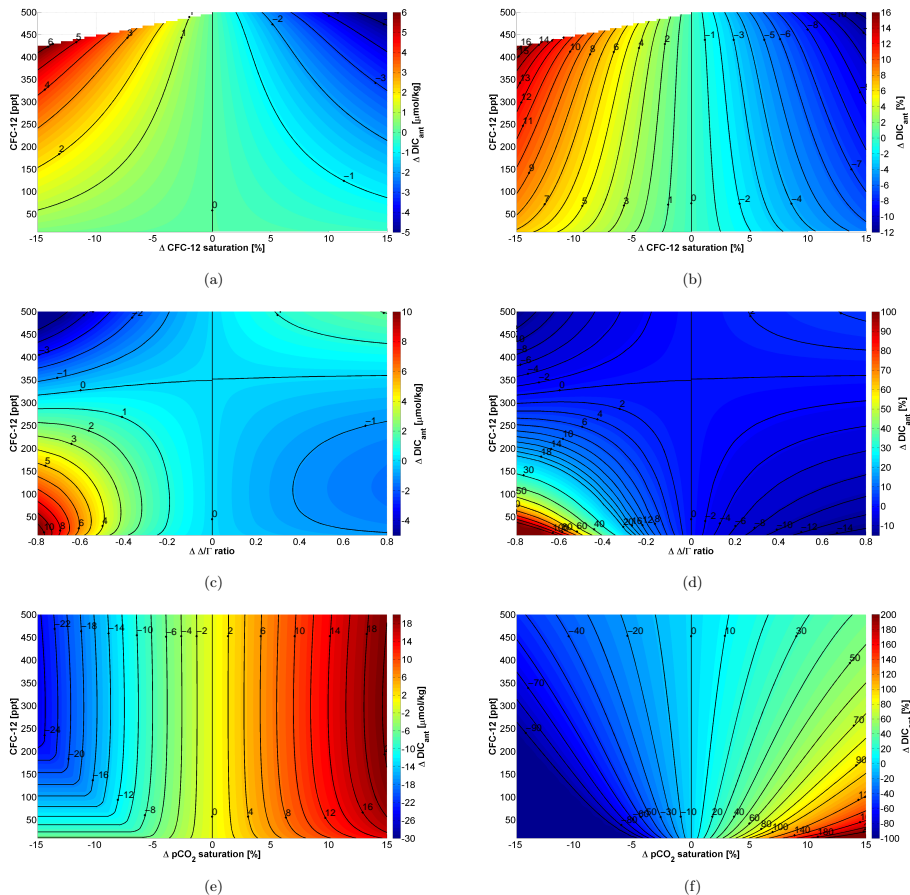


**Figure 12.** Anthropogenic carbon concentration sensitivities as a function of CFC-12 concentrations vs. changes in **(a, b)** CFC-12 saturation, **(c, d)**  $\Delta/\Gamma$  ratio and **(e, f)**  $p\text{CO}_2$  saturation. Deviations are stated in absolute (left panels) and relative (right panels) values. The reference points are defined by 100 % saturation of CFC-12 and  $p\text{CO}_2$  and a ratio of  $\Delta/\Gamma = 1.0$ .